

Improved Modeling and Control of a HTA Grid Connected 500 KW PV Systems

Ibrahim Benabdallah* and Adnene Cherif

Faculty of Sciences of Tunis El Manar, PB 2092, Belvedere, Tunisia; ibrahim.benabdallah@gmail.com, adnen2fr@yahoo.fr

Abstract

In this study, a grid connected PV system to a realistic HTA grid model is presented in details. **Objectives:** The main objective is the technical and quality evaluation of the grid integration of a 500 KW Photovoltaic station into a finite power grid model. **Methods/Statistical Analysis:** Two tasks are expected to be performed; firstly, the injection of maximum PV power return into Point Of Connection (POC) although respecting the tolerable variation in terms of voltage levels based on grid code. Undeniably, this amounts to simulate the suggested system with real components under a sudden climatic change. **Findings:** Therefore, performed studies may reveal power quality concerns, unlike the infinite impedance models of point of connection or the equivalent utility grid. Secondly, the flowing power quality and voltage levels are controlled at anytime and anywhere, through the grid. For this, we developed mathematical models of each part of the system from the PV arrays to the grid. This step allowed us to study the dynamic stability, then to establish suitable regulation and control laws for the DC/DC and DC/AC converters and finally to simulate the electrical signals from production to distribution by using MATLAB/SIMULINK environment. **Application/Improvements:** We obtained good satisfaction ratios and acceptable voltage levels without storage units using optimal monitoring strategy based on optimal power extraction and exchange between the PV Generator, grid and loads.

Keywords: Control, Finite Power, Grid Model, Modeling, PV System, HTA Grid Connected

1. Introduction

Over the last decades, the advancement in the solar industry implies a rapid decrease in the installation fees with competitive kW/H costs. Solar power has many application fields like electrification in standalone or grid connected systems, water pumping and air conditioning¹. Currently, applications of Grid-Connected Photovoltaic Systems (GCPVSs) have gained more attention compared to those electrifying isolated sites. Direct connection to the grid offers the privilege of getting rid of the expensive storage and maintenance problems. Traditional power system even it's incapable to deliver demanded powers in peak hours considering the significant demand growth for power consuming, it's considered as a stable system. Any massive introduction of energy sources causes instability around the Point

Of Connection (POC). This connection is based on strict requirements for active and reactive power, voltage stabilities, frequency and fault protective devices selectivity.

Many related works to the grid modeling are found in the literature. They could be classified as an equivalent three-phase voltage source or the venin equivalent circuit. Therefore, we consider that these types of modelling cannot provide a precise idea about the stability of the voltage levels and the state of power flows from the overall set.

The common interest of developed models is to overcome and assess many issues affecting PV-Grid interconnection such as over voltage, voltage drops, load demand-offer mismatch causing frequency deviation, grid failure and discontinuities, excessive DC link voltages, excessive AC currents in medium voltages and

*Author for correspondence

other aspects from the grid side like voltage and frequency instability and integration rate evaluations. In order to resolve these limitations many previous studies are developing new strategies of control and monitoring as in the Ref² Authors deployed solar inverters reactive power control inconvertibility. Their method is based on the grid voltage profile for location dependent PF set premium could be cushioned to whole solar inverter. Their main target was to alleviate unnecessary Q absorption. This method combines two droop function power factor active power and Q-(V) strategies. The performance of each inverter is to compare the output voltage measured and control the quantity of Q.

While in³ authors performed active power curtailment techniques in order to reduce the active power injected amount by the PV inverters. The inverter's bus voltage increases above a certain value. Consequently, it promotes the installed PV capacity and energy yield mean while preventing over-voltage. They investigate a number of approaches for sizing and controlling the PV power generated by 12 net-zero energy houses equipped with large rooftop PV systems in a typical 240 V/75 kVA Canadian suburban radial distribution feeder. One-year time with typical solar irradiance and load curves are presented to evaluate the performance of the different approaches in terms of overvoltage occasion, sharing of the trouble for overvoltage prevention per house and total energy yield of the residential PV feeder.

In⁴ the effectiveness of active and reactive power control of distributed PV inverter systems is discussed aiming to prevent over-voltage and improve network power quality. Hence, active power curtailment and reactive power injection control functions are presented.

While, in⁵ a centralized voltage control methodology presented considering that PVGs are reactive power providers. A new controller is presented based on self-adapting optimizing method controlling grid voltage in real time, under several burdensome events like overload, Under-load and generators tripping.

In⁶ they studied the participation of PVGs in the frequency regulation either by power curtailment in droop control mode or emergency control mode in severe faults acting on real power to alleviate the frequency overshoot. And in⁷⁻⁹ grids' fault failure is examined.

Furthermore, the necessity to ensure connection with a minimum of harmful effects in POC is an obligation prescribed by grid codes. In order to meet the require-

ments and standards of connection PV topology chains and commands must be adapted.

Many researchers studied the variants topology of a low/medium grid connected PV system. Single-stage and two-stage GCS are commonly used topologies in single and three-phase PVGCS;

Where in⁹, three phase single stage used to assess inverter disconnections under grid faults, excessive DC link voltages and excessive AC currents in medium voltages.

Single phase single stage inverter connected to low voltage grid used PQ theory and proportional resonant current control is presented in¹⁰ to mitigate the oscillation effect on the DC-link voltage.

Three phases' two stages Neutral Point Clamped (NPC) inverter connected to low voltage grid by an isolated DC-DC converter and using an Improved Practical Swarm Optimization (IPSO) is discussed in¹¹ to improve Low Voltage Ride Through (LVRT) and its transient behaviour limit by using a DC chopper circuit.

Two-stage grid connected PV system, using perturbation and observe Maximum Power Point Tracking (MPPT) technique, current and DC link voltage controllers¹². It demonstrated that the imbalance between the generated power and the load demand is due to a grid fault besides it could damage the DC-link capacitor.

Single phase two stage grid connected PV system, controlled by MPPT applied around the DC-DC converter and a current controller around the inverter¹³. Aim to alleviate the side effects of the double grid-frequency voltage ripple on the transferred power quality and the operational efficiency of the GCPVS.

Subsequently, Two main novelties are presented in our work as a first contribution we introduce later a detailed description of a global equivalent model from the production to the distribution grid and as a second novelty we improve the results of initial overshoot value while keeping a good response time by performing a PID control for the DC bus in order to improve the global system accuracy. On the PV conversion chain side, we will use a dual-stage backbone structure because of its simplicity at the implementation level. Thus, the two commands rated converters are uncorrelated to achieve¹⁴. In our case, the impedance adapter (Chopper) uses the ICMPTP incremental conductance enhanced high-frequency switching technique. At the output of the conventional control, an integral proportional regulator (PI) is inserted in order

to eliminate the induced power losses at the oscillations around the MPP point. An inverter with three-phase NPC-3-level topology is connected to the medium-voltage HTA network via a step-up transformer. A high frequency clock is applied to the inverter with three loops. The first loop regulates the DC bus at its nominal voltage by using a PID controller instead of the PI to ensure good stability and to minimize the overrun when switching on or setting up the connection. The first loop aims to control the injected currents into the grid. They have been taken from it as a reference to be reproduced. The last loop is requested to generate the three reference voltages equivalent to the number of phases. The latter two loops use PI regulators. An RLC filter, interposed between the inverter and the network, minimizes harmonic distortion and improves the quality of the synthesized signal.

This paper is divided into three main sections. Section II describes the configuration of the GCPVS. In section III system Modeling and methodology are discussed. The last section presents obviously the simulation results and discussions.

Configuration of The Grid Connected PV System

The GCPVS includes 5 similar PV Generators (PVG). Each generator is connected to a boost converter which is controlled by 5 kHz IICMPPT, followed by a PI loop to eliminate static error¹⁵. The system includes a DC capacitor that connects the output terminals of the boost to the inverter. Three-level, three-phase inverter, controlled by a 2 KHz SPWM signal is used to connect the DC with the AC part. An RCL-filter is used to couple inverter to the grid. It allows the smoothing of its current and purges unwanted generated harmonics. Step-up transformer raises voltage to 30 kV and interfaces low voltage to the POC voltage. The overall system configuration is given by Figure 1.

3. System Modelling and Methodology

3.1 Modelling of the Overall System

- Continuous part: The continuous part is composed by a GPV, DC-DC converter and DC bus, inspired from Refs¹⁶⁻¹⁸.

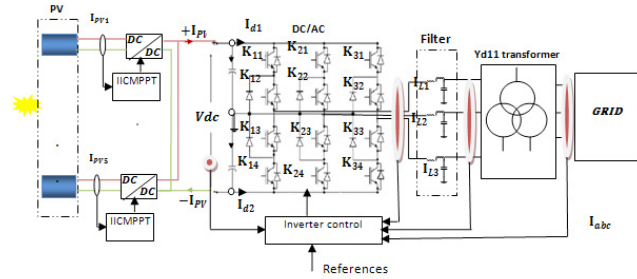


Figure 1. Block diagram of the grid connected GPV.

3.1.1 Modelling of GPV

PVG outputs, for either cell or array, are drawn taking into account the number of parallel and series cells. Every voltage is multiplied by the number of series cells n_s current by the number of parallel cells n_p and resistance by ns/n_p . According to the one diode electrical model adopted¹⁶, the PV current and voltage are given by the following equation:

$$\begin{cases} I_{PV} = I_{ph} - I_d - I_{rsh} \\ V_{PV} = R_{sh} * I_{rsh} - R_s * I_{PV} \end{cases} \quad (1)$$

$$I_{ph} = \left(\frac{E}{E_{ref}} \right) * [I_{phref} + \mu_{isc} (T_{cell_K} - T_{ref_K})] \quad (2)$$

$$I_d = I_{sat} * [e^{\frac{V_d}{V_i^{(t)}}} - 1] \quad (3)$$

$$I_{(sat_r)} = I_{(sat_{ref})} * \left(\frac{T_{cell_K}}{T_{ref_K}} \right)^3 * e^{\frac{(E_{gref} - E_g)}{(\sigma * T_{ref_K})}} \quad (4)$$

$$E_g = E_{gref} * \left(1 + \frac{dE_g}{dt} * (T_{cell_K} - T_{ref_K}) \right) \quad (5)$$

$$I_{rsh} = \frac{\left[\left(\frac{E}{E_{ref}} \right) * V_d \right]}{R_{sh}} \quad (6)$$

$$\left\{ \begin{aligned} V_d &= V_{pv} + R_s * I_{pv} \\ V_i(t) &= V_{tref} * \frac{T_{cell_K}}{T_{ref_K}} \\ V_{tref} &= \frac{K_B}{q * n * N_{cell/module} * N_{series/modules/string}} \end{aligned} \right. \quad (7)$$

I_{ph}: photo-generated current.

I_d: diode current.

Isat: saturation current [A].
 Eg: gap energy [J].
 Irsh: shunt resistance current [A].
 KB: Boltzmann constant.
 Tcell_K: cell temperature Kelvin [K].
 Tref_K: reference temperature in Kelvin [K].
 q=1.6*10⁻¹⁹ electron charge in coulomb[C].
 n: ideality factor.
 Ncell/module: number of PV-cells per module.
 Nseries modules/string: number of series PV-modules per string.

3.1.2 Modelling of the Boost Converter

Based on the dynamic operation mode of the boost converter, the equations governing its operation are given by¹⁸⁻¹⁹

$$\begin{cases} V_{out} = U_c = \frac{V_{pv}}{(1-\alpha)} \\ I_{out} = \frac{U_c}{R} = (1-\alpha) \cdot I_{in} = (1-\alpha) I_l \end{cases} \quad (8)$$

α : duty cycle
 R : equivalent load at output.

3.1.3 DC Bus Model

The capacity of DC bus is divided into two equal capacities in order to make a neutral point connectable at the entrance of inverter modeled with currents going through¹⁶⁻¹⁸:

$$\begin{cases} C_i \frac{dU_{ci}}{dt} = i_{Ci} \\ i = 1, 2 \\ i_{c1} = i_{pv} - i_{d1} \\ i_{c2} = i_{pv} + i_{d2} \\ i_{c0} = i_{c1} - i_{c2} \end{cases} \quad (9)$$

C_i: capacitor value.
 U_{ci}: voltage at capacitor terminals number i.

- Alternative Part

3.1.4 Inverter Modelling

We consider a three-phase inverter NPC type “Neutral-Point Clamped” controlled by PWM signal¹⁹⁻²¹. Voltages of three phases generated from the NPC inverter are expressed of bus voltage as follows:

$$\begin{cases} V_A = \frac{1}{3} \cdot (2 \cdot K'_1 - K'_2 - K'_3) \cdot U_{c1} - (2 \cdot K''_1 - K''_2 - K''_3) \cdot U_{c2} \\ V_B = \frac{1}{3} \cdot (-K'_1 + 2 \cdot K'_2 - K'_3) \cdot U_{c1} - (-K''_1 + 2 \cdot K''_2 - K''_3) \cdot U_{c2} \\ V_C = \frac{1}{3} \cdot (-K'_1 - K'_2 + 2 \cdot K'_3) \cdot U_{c1} - (K''_1 - K''_2 + 2 \cdot K''_3) \cdot U_{c2} \end{cases} \quad (10)$$

With:
 $K'_i = K_{i1} * K_{i2}$, $K''_i = K_{i3} * K_{i4}$, K is the IGBT
 Inverter output currents are given by these expressions:

$$\begin{cases} i_{L1} = K'_1 i_1 + K'_2 i_2 + K'_3 i_3 \\ i_{L2} = K''_1 i_1 + K''_2 i_2 + K''_3 i_3 \\ i_{L3} = (1 - K''_1 - K''_2) i_1 + (1 - K'_2 - K'_3) i_2 + (1 - K'_3 - K''_3) i_3 \end{cases} \quad (11)$$

3.1.5 Transformer Model

$$V_i = R_i * I_i + \sum_{k=1}^i L_{ik} * \frac{dI_{ik}}{dt} \quad (10), \quad i = 1, \dots, 6 \quad (12)$$

Where: R_i are the resistances of windings and L_{ii}, L_{ij} are self and mutual inductances. These parameters are calculated from tests either in short-circuit or open circuit applied to the transformer²¹.

3.1.6 RLC Filter Model

The filter model is governed by the transfer function per one phase:

$$H(p) = \frac{1}{1 + RCp + LCp^2} \quad (13)$$

The three-phase low pass second order filter has a cut-off frequency

$$\frac{1}{\sqrt{LC}} \quad \text{and a quality factor } Q = \frac{1}{RC\omega_0} = \frac{L\omega_0}{R}$$

3.1.7 Grid Model

The grid model drawn in Figure 2, here under consists of; a traditional voltage source station. This generator feeds a first step-down transformer modelling production HTB to repartition HTA “T1”. A sophisticate transformer “TN”, its main role is to generate the neutral wire. “L1PQ”, tied at POC90 (designing 90 KV). 10 km transmission line to

its terminals connected a second load “L2PQ”. A second step down Transformer T2 at POC30. In the secondary side connected two loads; “L3PQ” and after 8 Km feeder “L4PQ”. Last step-down transformer T3 at POC400. This voltage level represents low distribution grid. The PV plant generates 500KW power at STC. It is connected directly to 30KV at POC30. The grid model is inspired from Refs²²⁻²³ and their components are summarized in Table 1.

Line feeders used in this grid model are PI model lines taking into account interactions between wires, resistive, inductive and capacitive phenomenon²⁴.

Table 1. Parameters of Grid components

Element	Name	Voltage level (KV)	P (MW)	Q (MVAR)	S or SCC (MVA)
Source station	SS	135	-	-	2500
Transformer	T1	120 / 90	-	-	47
Grounding transformer	TN	90	-	-	47
Load1	L1PQ	90	20	5	20.6155
Load2	L2PQ	90	20	5	20.6155
Transformer	T2	90 / 30			47
Load3	L3Z	30	0.1	0	0.1
Load4	L4Z	30	0.5	0	0.5
Transformer	T3	30/0.4	-	-	47
Dynamic load	PV plant	0.4	0.5	0	0.5

3.2 System Commands

3.2.1 The MPPT control

Indeed, ICMPTT algorithm performs better than the P&O in a rapidly changing weather conditions. However, this is a slightly more complex algorithm to the implementation level. Nevertheless, not more complex than non-conventional methods like fuzzy logic algorithm or neuronal network method. It has good accuracy and uses both current and voltage sensors²⁵.

At the maximum power point

$$\frac{dP}{dV} = 0 \tag{14}$$

Which is equivalent to:

$$\frac{d(V \cdot I)}{dV} = 0 \Rightarrow I + \frac{V \cdot dI}{dV} = 0 \Rightarrow \frac{\Delta I}{\Delta V} = -\frac{I}{V} \tag{15}$$

The error $\frac{\Delta I}{\Delta V} = -\frac{I}{V}$ must tend towards 0 which is not the case in reality. The PI controller mentioned in Figure 3. The Output of $Re g_{pi}$ is also Correction of Duty Cycle (CDC). With CDC is the step size varying the duty cycle and must stay within the limit bounded¹⁸.

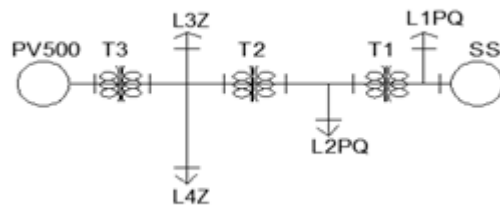


Figure 2. One-line diagram grid model.

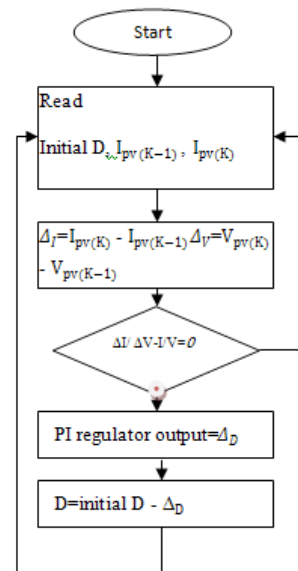


Figure 3. IICMPPT block chart.

3.2.2 Block Diagram of the Inverter’s Control

Inverter control is constituted from 3 loops.

3.2.2.1 DC link voltage control

In Figure 4, I_{dref} is synthesized using a PID controller tuned using forward Uler gathered with anti-wind up

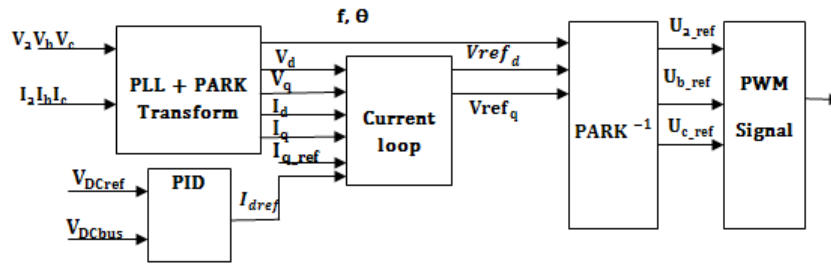


Figure 4. Inverter control.

algorithm. The PID eliminates the error between the bus voltage and its reference. The filtered derivative component overcomes the overshoot at the transient regime and bounds the overshoot in case of just PI controller.

3.2.2.2 PARK transforms and PLL

$$k1 = \frac{\sqrt{3}}{\sqrt{2 \cdot 30 \cdot 10^3}}, K2 = \frac{\sqrt{3} \cdot 30 \cdot 10^3}{\sqrt{2 \cdot 500 \cdot 10^3}}$$

In Figure 5, we get out from the PLL's output: frequency f and phase which are used to synthesize equations of voltages and currents governing park transformation. We apply the same method to carry out I_d, I_q et I_0 .

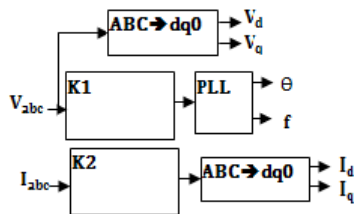


Figure 5. PLL and PARK transform.

3.2.2.3 Current loop

$$\begin{cases} Vd_{ref} = V''_d + Vd + R \cdot Id_{ref} - L \cdot Iq_{ref} \\ Vq_{ref} = V''_q + Vq + R \cdot Iq_{ref} + L \cdot Id_{ref} \\ V_0 = 0 \end{cases} \quad (16)$$

Figure 6 describes the voltage loop control using the filter equations in Park frame reference Vd_{ref}, Vq_{ref}, V_0 . With

$$V''_d = \frac{L \cdot dI_d}{dt}, \quad V''_q = \frac{L \cdot dI_q}{dt}$$

R is the total resistance composed of transformer and filter resistances. L is the total inductance which contains the transformer and the filter inductances. The control-

lers are tuned using the forward Euler algorithm gathered with anti-wind up method.

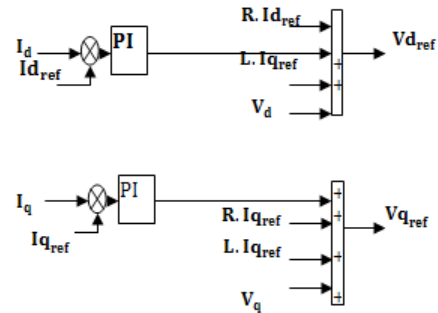


Figure 6. Current control loop.

3.2.2.4 Synthesizing Reference voltages

We manage reference voltages in the Park inverse frame taking into account all possible corrections:

$$\begin{cases} V_a = V_d \cdot \sin\left(\omega t + \varphi_d - \frac{11\pi}{6} + 2\pi f_n T_s\right) + V_q \cdot \cos\left(\omega t + \varphi_q - \frac{\pi}{6} + 2\pi f_n T_s\right) \\ V_b = V_d \cdot \sin\left(\omega t + \varphi_d - \frac{11\pi}{6} - \frac{2\pi}{3} + 2\pi f_n T_s\right) + V_q \cdot \cos\left(\omega t + \varphi_q - \frac{11\pi}{6} - \frac{2\pi}{3} + 2\pi f_n T_s\right) \\ V_c = V_d \cdot \sin\left(\omega t + \varphi_d - \frac{11\pi}{6} + \frac{2\pi}{3} + 2\pi f_n T_s\right) + V_q \cdot \cos\left(\omega t + \varphi_q - \frac{11\pi}{6} + \frac{2\pi}{3} + 2\pi f_n T_s\right) \end{cases} \quad (17)$$

$\left(\frac{-11\pi}{6}\right)$ In (17) is error correction due to transformer phase shifting, knowing its connection is YD11 and $2\pi f_n T_s$ is the sampling delay correction. Once we have references, we synthesize the 12 PWM control pulses.

4. Simulation Results and Discussion

We considered 5 PV generator connected in parallel every one provide 100.8 kW at its output. The single GPV consisting of 64 rows, each row is five identical modules connected in series ($64 \cdot 5 = 1600$ module used in this PV

field). The selected PV modules; Sun Power Type (SPR-315) with the specifications given in Table 3

Figure 7a and Figure 7b are registered as P_V curves for one PVG demonstrating generator Irradiation and Temperature variation impacts. These curves show the non-linear shape of the characteristic $P = f(V)$ and the influence of sunlight and temperature at the maximum power output. The simulated MPP agrees with the last one provided by the manufacturer and it's about 315 Wp for one module. Thus, we justify the maximum extracted power 100.8 kW for the GPV ($315 \times 64 \times 5$).

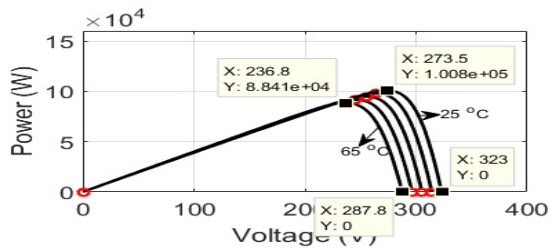


Figure 7b. Temperature impacts at 1000W/m².

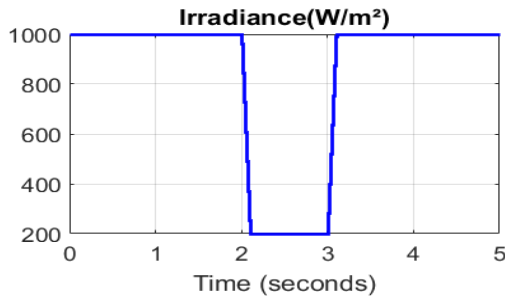


Figure 7c. Irradiation profile.

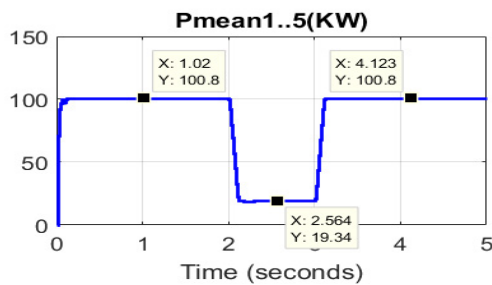


Figure 7d. PV generators mean power.

Figure 7c records the sunlight profile which we suppose that GPV is exposed to a uniform sunlight profile equivalent to a Cloud crossing Clear sky. In consequence, Irradiation decreases from 1000 w/m² to 200 w/m² dur-

ing the period 2 to 3 seconds. Otherwise stills constant 1000 w/m².

Figure 7d represents generated power by single GPV. It's about 100 KW at STC (1000 w/m² and 25°). Accordingly, 5 generators have to produce 500 KW at STC against 96.75 (19.35*5) when irradiation is 200 w/m². It can be noted that irradiation varies and mean power tracks sunlight profile.

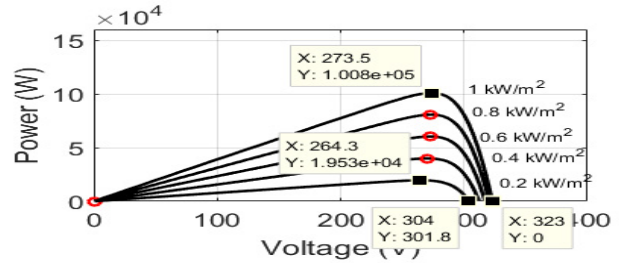


Figure 7a. Irradiation impacts at 25°C.

At $t = 0.02s$ controls are unlocked. Power reaches its MPP in accordance with irradiation. Figure 8a depicts the DC bus voltage set point has been reached within 0.13s thanks to the PID action. From 0.13 s to 2 s the voltage remains unchanged 500V. It retains its value after 0.2s which is the necessary time for controls response. The sudden change in irradiation curve induces a drop in DC bus at ($t=2s$) and a raise at ($t=3s$).

In comparison with [1] we extenuate the overshoot to 622 v against 700 V for five times their generated power (500 Kw) at price of response time (0.13 against 0.1007s) which is insignificant for a climate change.

Figure 8b shows the evolution of the mean errors in output of boost controllers. Reveling a fast responding time in addition, we justify PI regulator action which vanishes error.

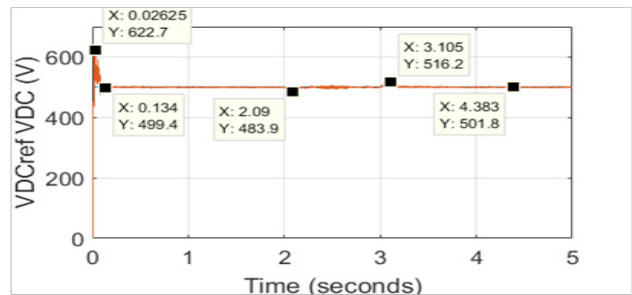


Figure 8a. DC-link reference and measured voltage.

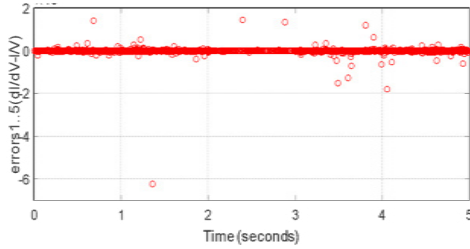


Figure 8b. DC-link Reference and measured voltage.

In Figure 9a I_d and I_{dref} are merged and been worth 0.8 per unit against 0 for the reactive current in Figure 9b. Thus, we attempt to have only active power flow on POC. Figure 9c Represents U_{aref} , U_{bref} , U_{cref} , which are reference voltages applied to the pulse generator to synthesize the corresponding PWM signals.

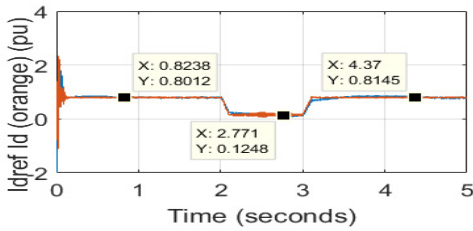


Figure 9a. Reference and measured direct current.

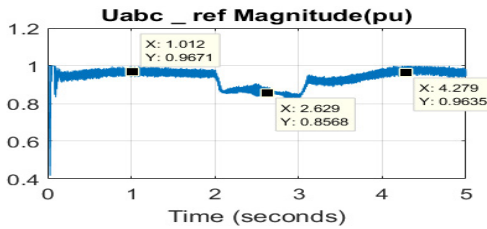


Figure 9b. Quadratic current.

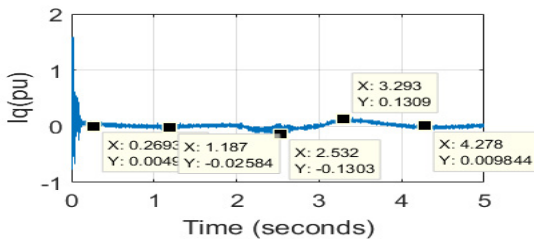


Figure 9c. Reference voltages magnitude.

Figure 10 presents the received power at POC is 485 KW from 500 KW sent. This means a yield of 97% at STC. As a consequence; clouds prevent the luminous flux and seriously decreasing it. Irradiation falls from 1000 W/m^2 to 200 W/m^2 . It implies a decrease from 487 KW to 93 KW. It's noticeable that 30 KV voltage and current are in

phase, due to the fact that loads tied at this part are resistive, revealing a good power factor close to unity. As well as voltages, currents modulus remains perfectly stable within regulatory limits.

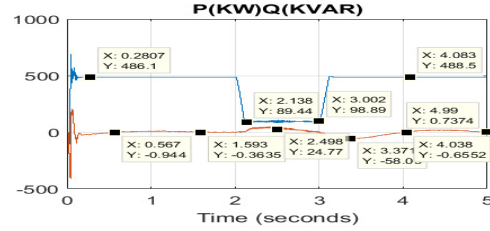


Figure 10. Power at POC.

In Figure 11a and Figure 11b respectively. The voltage at POC is constant in spite of intermittent of sunlight. Furthermore, within acceptable bounds value (nominal voltages $\pm 5\%$) even in sudden changes 29.91 KV at 2.1s or 30.04 KV at 3.1s. Current at POC varies from 10A (1000 W/m^2) to 2A (200 W/m^2) dependently from irradiation.

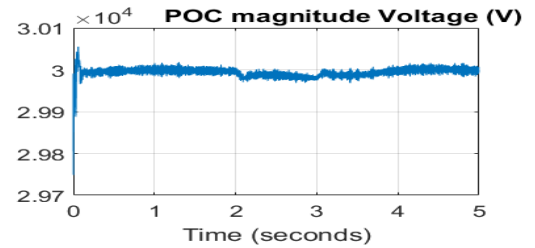


Figure 11a. Voltage at POC30.

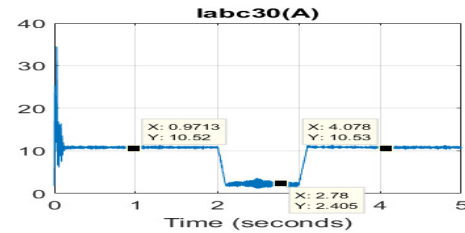


Figure 11b. Current at POC30.

Figure 12a and Figure 12b Shows 90 KV voltage and current in the repartition part of the grid. We notice that the voltage remains immunized toward GED intermittent.

Figure 13a and Figure 13b are the characteristics of the voltage levels in the production grid part. We have an oversized conventional source in order to maintain 90 KV and 30 KV voltage stages stable. The source delivers 133 KV constant moreover, current is slightly variable from

343.9A to 346A subsequently on load demand. In Figure 14, frequency control action stabilized quickly in less than 0.2 s and is performing grid requirements.

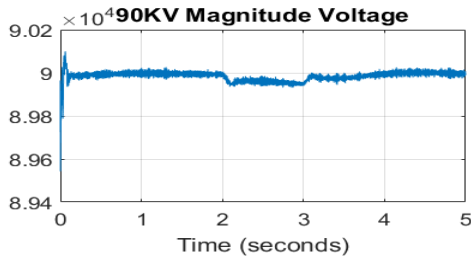


Figure 12a. Voltage at POC90.

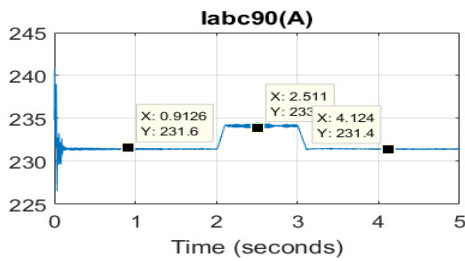


Figure 12b. Current at POC90.

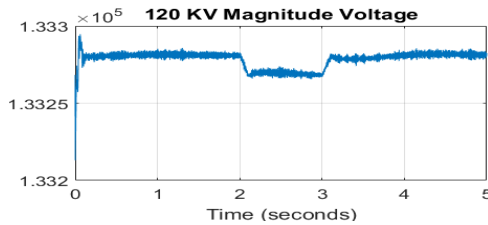


Figure 13a. Voltage at POC133.

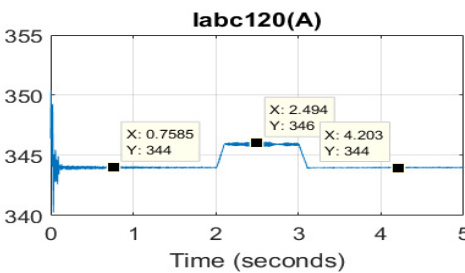


Figure 13b. Current at POC120.

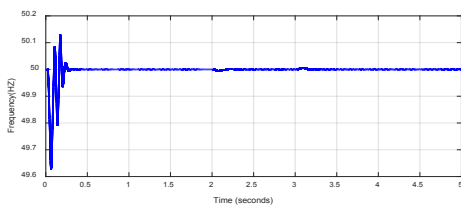


Figure 14. Frequency variation.

To validate our simulation results we opt experimental results for grid part from²⁶. Hereunder a comparison between both electrical network characteristics: 400 V (for LV), 30 KV, 60 KV (HTA), 133 KV (HTB) in Table 2 are imposed by the Tunisian grid operator²⁷⁻²⁸.

Prams used for the modeling of PVG are listed in Table 3.

Table 2. Comparison of Grid components

	Grid characteristics[28]	Presented Grid characteristics
Low voltage(LV)/ medium voltage(MV)	4MVA, 25/0.6KV,ecc=7.7%	47MVA, 30/0.4KV,ecc=7%
MV lines	r=0.115Ω/KM ,x=0.33 Ω/KM, length=1Km	r=0.1153Ω/KM, x=0.32Ω/KM, length=10Km
MV Cluster lines	r=0.115Ω/KM ,x=0.33 Ω/KM, length=25Km	r=0.1153Ω/KM, x=0.32 Ω/KM, length=8Km
MV/HV transformers	47MVA, 25/120KV,ecc=3.3%	47MVA, 30/133KV,ecc=3%
Grid short circuit power	2500MVA X/R ratio=10	2500MVA X/R ratio=7

Table 3. GPV System parameters

Array	
Number of series modules per string	N _{sm} =5
Number of parallel strings	N _{ps} =64
Module	
Short circuit current	I _{sc} = 6.14 A
Open circuit voltage	V _{co} = 64.6 V
Maximum power point current	I _{pm} = 5.76 A
Maximum power point voltage	V _{pm} = 54.7 V
Temperature coefficient of V _{oc}	μTV _{oc} cell%/°c = -0.27269
Temperature coefficient of I _{sc}	μTI _{sc} cell%/°c = -0.061694
Photo generated current	I _{phref} = 6.1461 A
Diode saturation current	I _{satref} = 6.5043 e-12 A
Series resistance	R _s = 0.43042 Ω
Shunt resistance	R _{sh} = 430.0559 Ω

5. Conclusion

This paper highlights the study of the grid connected three-phase electrical systems to medium voltages. We presented the different mathematical models as well as a detailed dynamic study of its behavior is recorded. The efficiency and life expectancy of all components of the system were implicitly lifted up by the appropriate control laws that yield to the desired efficiency. The optimization of energy transfer with good signal quality is ensured with the multi-level inverter. The network equivalent model is generally presented as an equivalent source that is not being able to qualify the stability of the grid in terms of voltage level and the frequency predefined by the network code. To overcome this leakage, we have introduced a detailed network model that allows us to evaluate the entire system from production to distribution.

6. References

1. Petrakopoulou F, Robinsonc A, Loizidou M. Simulation and evaluation of a hybrid concentrating-solar and wind power plant for energy autonomy on islands. *Renewable Energy*. 2016 Oct; 96(A):863–87.
2. Darwish EM, Hasanien HM, Atallah A, El-Debeiky S. Reactive power control of three-phase low voltage system based on voltage to increase PV penetration levels. *Ain Shams Engineering Journal*. 2017:1-7.
3. Tonkoski R, Lopes LAC. Impact of active power curtailment on over voltage prevention and energy production of PV inverters connected to low voltage residential feeders. *Renewable Energy*. 2011 Dec; 36(12):3566–74. Crossref
4. Collins L, Ward JK. Real and reactive power control of distributed PV inverters for over voltage prevention and increased renewable generation hosting capacity. *Renewable Energy*. 2015 Sep; 81:464–71. Crossref
5. Cangnano A, Tuglie ED. Centralized voltage control for distribution networks with embedded PV systems. *Renewable Energy*. 2015 Apr; 76:173–85. Crossref
6. Xin H, Liu Y, Wang Z, Gan D, Yang T. A new frequency regulation strategy for photovoltaic systems without energy storage. *IEEE Transactions Sustainable Energy*. 2013 Oct; 4(4):985–93. Crossref
7. Yang Y, Blaabjerg F. Low voltage ride-through capability of single stage single phase photovoltaic system connected to the low voltage grid. *International Journal of Photoenergy*. 2013:1–9. Crossref, Crossref, Crossref
8. Lin F-J, Lu K-C, Ke T-H. Probabilistic wavelet fuzzy neural network based reactive power control for grid-connected three-phase PV system during grid faults. *Renewable Energy*. 2016 Jul; 92:437–49. Crossref
9. Mirhosseini M, pou J, Agelidis VG. Single stage inverter based grid connected photovoltaic power plant with ride through capability over different types of grid faults. *IECON 39th Annual Conference of the IEEE Industrial Electronics Society; Vienna, Austria*. 2014 Jan. p. 1–6.
10. Brahim M, Blehadj J. Performance of PV grid connected system under grid failure. *International Journal of Renewable Energy Research*. 2013; 3(4):754–62.
11. Saad NH, El-Sattar AA, Mansour AEM. Improved particle SWARM optimization for photovoltaic system connected to the grid with low voltage ride through capability. *Renewable Energy*. 2016 Jan; 85: 181–94. Crossref
12. Hamrouni N, Jraidi M, Cherif A. New control strategy for 2-stage grid-connected photovoltaic power system. *Science directs Renewable Energy*. 2008 Oct; 33(10):2212–21. Crossref
13. Salem M, Atia Y. Control scheme towards enhancing power quality and operational efficiency of single-phase two-stage grid-connected photovoltaic systems. *Journl of Electrical Systems and Information Technology*. 2015 Dec; 2(3):314–27. Crossref
14. Ahmed MES, Orabi M, Abdel Rahim OM. Two-stage micro-grid inverter with high-voltage gain for photovoltaic applications. *IET Power Electronics*. 2013 Nov; 6(9):1812–21. Crossref
15. Lee JH, Bae H, Cho BH. Advanced incremental conductance MPPT algorithm with a variable step size. *12th International Power Electronics and Motion Control Conference; Portoroz, Slovenia*. 2009. p. 603–7.
16. Hoque A, Wahid KA. New mathematical model of a Photovoltaic Generator (PVG). *Journal of Electrical Engineering*. 2000 Jun; 28(1).
17. Sera D, Teodorescu R, kerekes T. Teaching maximum power point trackers using a photovoltaic array model with graphical user interface. *International Workshop on Teaching Photovoltaics*; 2006 Jan. p. 1–6.
18. Ben Abdallah I, Jraidi M, Hamrouni N, Cherif A. Modelling, control and simulation of a grid connected PV system. *IEEE Proceedings of International Conference, Electrical Sciences and Technologies in Maghreb (CISTEM); Tunisia*. 2014. p. 1–8.
19. Kolsi S, Samet H, Amar MB. Design Analysis of DC-DC converters connected to a photovoltaic generator and controlled by MPPT for Optimal energy transfer throughout a clear day. *Journal of Power and Energy Engineering*. 2014 Jan; 2(1):27–34. Crossref
20. Bouchafaa F, Aissa C, Boukhalfa S. Stability of input voltages of a three-level inverter NPC fed by photovoltaic sources. *Revue des Energies Renouvelables*. 2012; 15(3):501–12.
21. Labrique F, Seguier G, Bausiere R. *Les Convertisseurs de l'électronique de puissance, La conversion continu – alternatif*. 2nd editon. 1995 Sep.

22. Almi MF, Arrouf M, Belmili H, Bendib B. Contribution to the protection of PVG connected to three phase electrical network supply. *Energy Procedia*. 2012; 18:954–65. Crossref
23. Brandwajn V, Donnel HW, Dommel I I. MATRIX representation of three-phase n-winding transformers for steady-state and transient studies. *IEEE Transactions on Power Apparatus and Systems*. 1982 Jun; 101(6):1369–78. Crossref
24. Semlyen A, Deri A. Time domain modelling of frequency dependent three- phase transmission line impedance. *IEEE Transactions on Power Apparatus and Systems*. 1985; 104(6):1549–55. Crossref
25. Verman D, Nema S, Shandilya AM, Dash SK. Maximum Power Point Tracking (MPPT) techniques: Recapitulation in solar photovoltaic systems. *Renewable and Sustainable Energy Reviews*. 2016 Feb; 54:1018–34. Crossref
26. Pardalos PM, Rebennack S, Pereira MVE, Iliadis NA, Pappu V. *Hand book of Wind Power Systems*. Berlin, Heidelberg: Springer-Verlag; 2013. Crossref
27. Analysis of the regulatory framework governing network access for producers of electricity from renewable energy sources in Tunisia. 2017. Available from: <https://www.giz.de/en/downloads/giz2014-en-renewable-energy-resources-tunisia.pdf>
28. Development project by the private sector of grid connected wind energy in Tunisia, development of institutional and regulatory framework. 2017. Available from: <http://www.prod2020.com>